CHAPTER EIGHT

Recent Advances in the Development of PET and SPECT Tracers for Brain Imaging

Lei Zhang, Anabella Villalobos
Pfizer Worldwide Research and Development, Neuroscience Medicinal Chemistry, Cambridge, Massachusetts, USA

Contents

1. INTRODUCTION

Positron emission tomography (PET) and single photon emission computed tomography (SPECT) are radiotracer-based noninvasive imaging techniques that provide quantitative binding information on specific target areas of interest.[1,2] PET and SPECT have been proven to be particularly valuable for imaging targets in the central nervous system (CNS) due to inaccessibility of the human brain, providing impact at various stages of the drug discovery process, from informing basic pharmacology to enabling critical decision-making in clinical evaluations of novel pharmaceuticals. To enable PET and SPECT brain imaging, suitable

Annual Reports in Medicinal Chemistry, Volume 47
ISSN 0065-7743
http://dx.doi.org/10.1016/B978-0-12-396492-2.00008-4

radiotracers need to be developed. Such processes, however, can often be arduous and lengthy due to the challenge of meeting a demanding set of prerequisite attributes for a tracer.[3] In this review, we will compare these two imaging modalities, highlight recent advances in CNS PET tracer development, and review recent data in the field of SPECT in brain imaging.

2. PET AND SPECT

While PET and SPECT bear similarities in their functions in brain imaging, they have their own strengths and limitations. In terms of radionuclides (Table 8.1), PET requires positron-emitting radionuclides such as [^{11}C] and [^{18}F], while SPECT requires gamma-emitting radionuclides such as [^{123}I] and [^{99m}Tc]. Routinely used PET radionuclides such as [^{11}C] and [^{18}F] are isotopes of elements commonly found in drug-like molecules that can be incorporated into these molecules with minimal impact on their physicochemical and pharmacological properties. Thereby, these radionuclides offer greater flexibility in tracer design in comparison to SPECT radionuclides which may result in modification of physicochemical and pharmacological properties upon incorporation into molecules. On the other hand, the shorter half-lives of PET radionuclides, [^{11}C] ($T_{1/2}$ = 20 min) and [^{18}F] ($T_{1/2}$ = 110 min), constitute a disadvantage in that rapid synthesis/purification as well as proximity to a cyclotron facility is required for their successful preparation. In comparison, SPECT radionuclides, such as [^{123}I] ($T_{1/2}$ = 13 h) and [^{99m}Tc] ($T_{1/2}$ = 6 h), have relatively longer half-lives and can be bought commercially or synthesized onsite with

Table 8.1 PET and SPECT radionuclides

PET radionuclides	$T_{1/2}$	SPECT radionuclides	$T_{1/2}$ (h)
^{11}C	20 min	^{99m}Tc	6
^{18}F	110 min	^{123}I	13
^{13}N	10 min	^{201}Tl	73
^{15}O	2 min	^{67}Ga	78
^{64}Cu	12.8 h	^{111}In	68
^{68}Ga	68 min	^{133}Xe	127
^{82}Rb	1.3 min	^{131}I	192

low-cost generators, thus offering more flexibility in tracer synthesis, lower cost, and better access to the technique.[4] In terms of brain imaging, currently PET offers superior spatial resolution (as low as 1.2 mm) and sensitivity to allow quantification of tracer concentration in brain regions of interest with higher degree of accuracy. In contrast, SPECT has lower spatial resolution (~10–14 mm) and sensitivity (2–3 orders of magnitude lower than PET). This drawback in sensitivity mainly stems from the limited geometry efficiencies of SPECT collimators which can only detect photons within a small angular range, thus recording a smaller percentage of emission events. In addition, both spatial resolution and sensitivity of SPECT are position dependent, with increased attenuation and scattering of the signal as it travels through the body and dense tissues. Therefore, SPECT, in general, requires a larger number of attenuation corrections and longer scan times, often yielding noisier images that are more challenging to quantify.[5]

3. CNS PET TRACERS: GENERAL REQUIREMENTS AND KEY HURDLES

There are many criteria that must be met by successful PET ligands. From a chemical structure point of view, a PET tracer should have functional groups that allow for rapid radiolabeling to accommodate the short half-lives of PET radionuclides. In terms of pharmacology, a PET tracer must be highly potent and selective toward its intended pharmacological target, which often requires subnanomolar potency and greater than 100-fold selectivity over other targets. In terms of metabolism, tracers that form permeable radioactive metabolites should be avoided to prevent confounding quantification results as the PET detector measures total radioactivity without distinction of origin. In addition to the aforementioned criteria, a suitable PET tracer also needs to be brain permeable and must have low nonspecific binding (NSB) to achieve requisite signal-to-noise ratio. In fact, poor brain permeability and high NSB are the most frequent causes for failure in CNS PET ligand development.[6] Historically, lipophilicity parameters such as $\log P$ and $\log D$ have been used as criteria to predict brain permeability and NSB. A general notion within the PET field is that lower lipophilicity typically leads to lower NSB, yet lipophilicity needs to reside in a certain range (e.g., $\log P$ 1.5–2.5 or $\log D$ 1–3) in order to retain brain permeability.[7,8] This over simplified approach, however, has not been sufficient to predict PET tracers performance *in vivo*. Furthermore, the rather narrowly defined ranges of

such parameters significantly restrict the scope of potential substrates for PET tracer development. Therefore, deeper understanding of molecular properties that are required for optimum brain permeability and low NSB as well as new research tools and assays that predict these two important parameters *in vivo* will likely provide significant impact in improving the overall efficiency of the CNS PET development process.

4. RECENT ADVANCES IN CNS PET TRACER DEVELOPMENT

4.1. Approaches to predict *in vivo* NSB

A biomathematical modeling approach to predict *in vivo* performance of PET radiotracers has been reported.[9] This method estimates the coefficients of variation of binding potential (%COV$[BP]_{ND}$), through Monte Carlo simulations based on *in silico* and *in vitro* physicochemical and pharmacological properties of candidate PET molecules including lipophilicity, molecular volume, free fractions in plasma and tissue, target density, affinity, perfusion, capillary surface area, and apparent aqueous volume in plasma and tissue. The performance of this approach was evaluated against a dataset containing 28 candidate PET tracers with preclinical *in vivo* endpoints available for comparison. In general, ranking of the tracers was consistent with their performance *in vivo*, with lower %COV$[BP]_{ND}$ values generated for clinically proven tracers such as [^{11}C]flumazenil and [^{11}C]raclopride and higher values observed for poor performing tracers such as [^{11}C]PK11195 and [^{11}C]GR205171.

Several methods evaluating the affinity of ligands for lipid membranes have also been reported as approaches to predict NSB. A high-throughput electrokinetic chromatography (EKC) method was developed based on a concept that the NSB of a given radiotracer primarily arises from its interaction with lipid cell membranes.[10] Three liposome and one surfactant vesicle systems were explored as *pseudo*-stationary phases to estimate membrane affinity of candidate molecules. Results indicated that the EKC analysis associated with an AOT (docusate sodium salt) vesicle system was shown to be the best approach, offering short run times, low cost, high reproducibility, and, importantly, a statistically significant correlation of retention times with *in vitro* or *in vivo* measured NSB parameters. Based on a similar tracer-lipid membrane interaction concept, an *ab initio* method showed a good correlation of the calculated drug–lipid interaction energy E_{int} with the *in vivo* measured NSB values of 10 clinically validated PET tracers.[11] A recent publication from

the same group further validated this hypothesis by expanding the validation dataset to a set of 22 new candidate CNS PET tracers.[12] Full *ab initio* quantum mechanical calculations appear to be necessary for a successful correlation as further attempts to speed up the calculation using several semiempirical methods failed to reproduce the correlation. This might limit the use of this method as a virtual screen tool due to slow computational processes. Recently, a similar correlation between *in vivo* specific binding (BP_{ND}) and compound–membrane interactions (K_m) measured by immobilized artificial membrane chromatography was reported using a validation set consisting of 10 known tracers. Higher K_m values were shown to correlate with lower BP_{ND} values, thus higher *in vivo* NSB, and $K_m \leq 250$ was proposed as a preferred range to prioritize compounds for tracer development.[13] Furthermore, correlation of *in vivo* brain permeability with additional *in vitro* HPLC-measured properties, such as lipophilicity ($\log P$), permeability (P_m), and plasma protein binding (PPB), was also explored using the same validation set. The results demonstrated that $\log P$ was not a reliable predictor for brain permeability, whereas a stronger correlation was observed with high P_m and a specific range of PPB (45–85%).

4.2. Design and selection parameters for PET tracer development

In another approach to increase the ability to predict brain permeability and NSB and enable the selection of successful PET tracers in an accelerated way, a systematic analysis of a dataset containing 62 clinically validated PET tracers and 15 failed tracers due to high *in vivo* NSB was carried out. The intent of this analysis was to define a desired property space for CNS PET tracers based on key differences between successful and failed tracers with respect to physicochemical properties and *in vitro* ADME endpoints.[14] For analysis of the physicochemical properties, a simple multiparameter optimization design tool (CNS MPO Desirability Score) was used to assess drug-like and brain penetration properties of tracers in the dataset.[15] The CNS MPO helps assess the alignment of six fundamental physicochemical properties that lead to drug-like, brain penetrant molecules and offers greater flexibility in CNS compound design beyond the use of single parameters or hard cutoffs. The *in vitro* ADME endpoints examined included human and rat liver microsomal clearance, RRCK Papp permeability, MDR1 (P-gp) efflux, and fraction unbound in brain (Fu_b) and plasma (Fu_p). Based on this analysis, in addition to the existing knowledge of *in vitro* pharmacology and selectivity criteria ($B_{max}/K_d > 10$ and selectivity $> 30\times - 100\times$), a

set of preferred design and selection parameters for a successful PET tracer were proposed. In terms of physicochemical properties, CNS MPO desirability scores >5 (CNS MPO2 >3)[16] and/or $\log D \leq 3$ should be targeted in the design and selection of PET ligands. In terms of PK parameters, RRCK Papp AB $>5\times10^{-6}$ cm/s for moderate to good passive permeability, MDR1 BA/AB <2.5 for low P-gp liability, and cFu_b (calculated fraction unbound in brain) >0.05 and cFu_p (calculated fraction unbound in brain) >0.15 for low risk of *in vivo* NSB should be targeted. This set of defined parameters was further evaluated against the profiles of 10 top performing CNS PET tracers selected based on their frequency of use, acceptance in the field, robust test–retest reliability, and good properties for quantification. This set of top performing tracers showed good alignment with the criteria defined above, suggesting that the above design and selection parameters could have the potential to steer novel CNS PET ligand development efforts toward higher performing ligands rather than marginal performers.

5. NEW CNS PET TRACERS

In the past year, a number of novel PET tracers for several hotly pursued targets in the pharmaceutical industry have been disclosed, driven by the increased use of PET imaging in clinical development to define receptor or target occupancy, exposures associated with efficacy, and dose selection. A better understanding of design principles; availability of chemical matter with suitable attributes such as better potency, selectivity, and brain permeability; and more efficient radiolabeling methodologies have also led to an increase in the development of novel PET ligands. New PET tracers developed for three targets, PDE10a, ORL-1, and FAAH, were selected to illustrate the important advances in the PET field.

5.1. PDE10a PET tracers

Phosphodiesterase 10a (PDE10a) is a unique dual specificity enzyme that hydrolyzes both cAMP and cGMP and plays a key role in regulating cyclic nucleotide signaling cascade. A suitable PET tracer would allow molecular imaging of the PDE10a enzyme in living subjects and facilitate the assessment of PDE10a as a drug target for various CNS disorders. The first reported PDE10a PET effort was the radiosynthesis and *in vivo* microPET evaluation of [^{11}C]-labeled papaverine (**1**), an early PDE10a inhibitor with moderate potency and selectivity.[17] While initial higher accumulation was

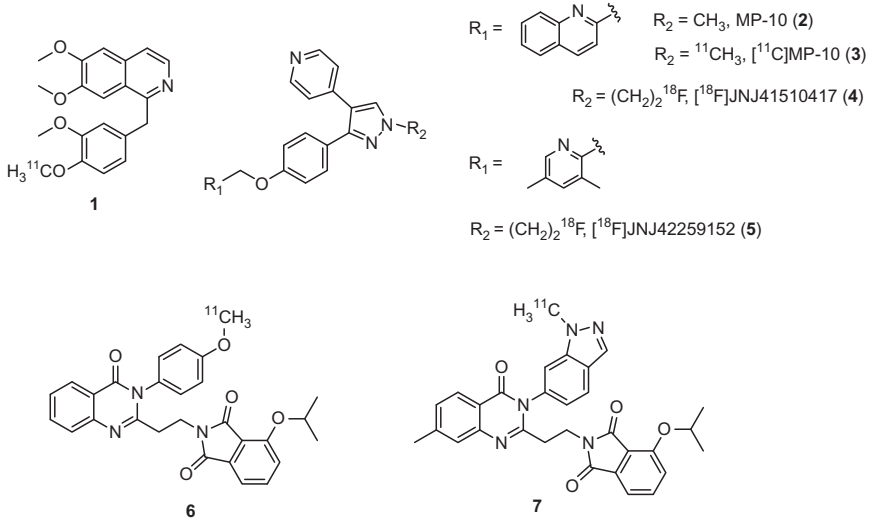

Figure 8.1 Structures of PDE10a PET tracers.

observed in striatum, a PDE10a-enriched region, the rapid washout in both rats and rhesus monkeys indicated that **1** was not a suitable PET tracer. Following the publication of a highly potent and selective PDE10a inhibitor MP-10 (**2**), several reports of novel PET tracers based on this chemotype emerged recently (Fig. 8.1). Recently, two research groups reported the development of [^{11}C]MP-10 (**3**) radiolabeled at the *N*-methyl of the central pyrazole ring.[18,19] Rapid brain uptake and preferential binding to striatum were observed with maximum striatum-to-cerebellum ratio of 6.55 and 1.5–2 in rats and rhesus monkeys, respectively. Similar brain uptake and preferential striatal binding were observed in porcine and baboons as well. Interestingly, while **3** achieved equilibrium in baboons roughly 40–60 min post dose, in rhesus monkeys, **3** showed continuous accumulation in striatum and cerebellum and did not reach equilibrium even at 120 min post dose. Metabolite analysis revealed the extensive formation of a brain permeable lipophilic radioactive metabolite in monkey, which may limit the clinical utility of **3**. Meanwhile, two [^{18}F]-labeled PET tracers derived from analogs of **2** were reported. A *N*-[^{18}F] fluoroethyl pyrazole derivative [^{18}F]JNJ4150417 (**4**) was found to have high PDE10a affinity ($p\mathrm{IC}_{50} = 9.3$) and showed specific and reversible binding to PDE10a in rats (peak striatum-to-cerebellum ratio of 4.6). However, the high lipophilicity ($C\log P = 4.2$) and exceptionally high protein binding in plasma (99.5%) of **4**, coupled with its high affinity,

led to undesirable slow kinetics.[20] Subsequent efforts aimed at the optimization of lipophilicity and affinity by replacing the 2-quinoline with more polar monocyclic pyridines yielded a superior radiotracer [^{18}F] JNJ42259152 (**5**) with lower lipophilicity ($C\log P = 3.66$) and sufficient affinity ($p\mathrm{IC}_{50} = 8.8$).[21] In rats and monkeys, **5** showed not only higher striatum-to-cerebellum ratios but also faster kinetics. The favorable overall profile positioned **5** to enter a first-in-human study for clinical PET imaging of PDE10a. However, it is worth noting that similar to **3**, brain permeable radioactive metabolites were also detected with **5**. Therefore, there is still a need for additional PDE10a PET tracers that are free of such metabolite issues. In addition to the MP-10-based PET tracers described above, two [^{11}C]-labeled PDE10a PET tracers **6** and **7**, from an alternative 4-oxo-3,4-dihydroquinazoline chemotype, were recently disclosed in the patent literature.[22] Cold reference compounds of **6** and **7** are highly potent PDE10a inhibitors with K_i values of 0.15 and 0.024 nM, respectively. The *in vivo* imaging results of these tracers were not discussed in the patent and have yet to be disclosed. It would be interesting to see whether tracers based on this alternative chemotype would offer differentiation in their metabolic profile, thereby minimizing the brain permeable radioactive metabolite issues associated with MP-10-derived PET tracers.

5.2. ORL1 PET tracers

Opioid receptor-like 1 (ORL1) receptors, also known as nociceptin/orphanin FQ peptide receptors, are widely expressed in CNS with potential links to many neuropsychiatric disorders. Development of a suitable PET tracer for the ORL1 receptor has been challenging due to its low expression level (B_{max}) and the high lipophilicity of literature leads. The first successful ORL1 PET tracer, [^{11}C]-(*S*)-3-(2′-fluoro-4′,5-dihydrospiro[piperidine-4,7′-thieno-[2,3-*c*]pyran-1-yl]-2(2-fluorobenzyl)-*N*-methylpropanamide (**8**), was reported in 2011 (Fig. 8.2).[23] Through structure–activity relationship (SAR) investigations around the amide alkyl chains and benzyl substitutions and subsequent *ex vivo* LC–MS/MS measurement in rats, **8** was identified as the best lead with potent ORL1 affinity ($K_i = 0.15$ nM) and preferential uptake in ORL1-rich brain regions. Baseline imaging in monkeys revealed good brain uptake and a brain biodistribution consistent with that expected of the ORL1 receptor. Importantly, the radioactivity in ORL1-rich brain regions could be blocked by predosing with a high dose of naloxone, an opiate receptor antagonist, confirming the specificity of **8** to

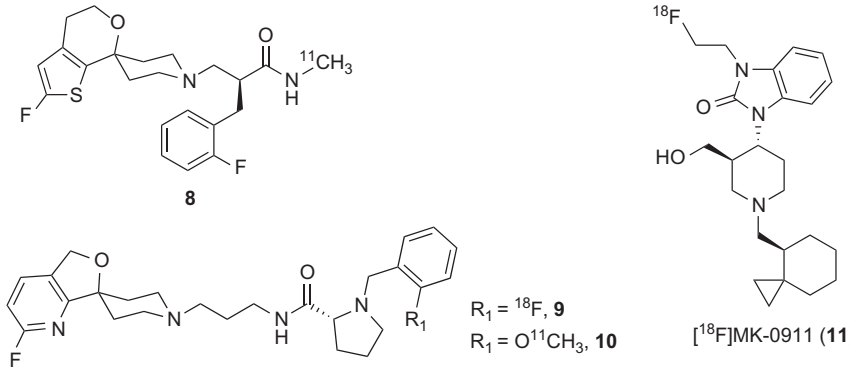

Figure 8.2 Structures of ORL PET tracers.

ORL1 receptor *in vivo* with an estimated specific to nonspecific ratio of 1.28 [30–90 min brain average area under the curve]. More recently, the characterization of several radiolabeled ORL1 antagonists (Fig. 8.2) were reported.[24] Analogs in a structurally similar spiropiperidine series, **9** ($IC_{50} = 0.54$ nM) and **10** ($IC_{50} = 0.71$ nM), though potent *in vitro*, showed poor brain permeability potentially due to high P-gp efflux (ratio > 3). In comparison, a structurally distinct benzo[*d*]imidazolone [^{18}F]MK-0911(**11**) showed low P-gp efflux (P-gp ratio = 1.4) while retaining favorable potency ($IC_{50} = 0.56$ nM), which nicely translated into high brain uptake and preferential binding in ORL1 enriched brain regions in monkey microPET imaging studies. The brain binding of **11** was blocked by a selective ORL1 antagonist MK-0584 in a dose-responsive manner, with a specific to nonspecific ratio of ~2, achieved at the high dose of MK-0584. The favorable profiles of **8** and **11** suggest that they may be suitable PET tracers for imaging ORL1 receptor in humans.

5.3. FAAH PET tracers

The fatty acid amide hydrolase (FAAH) enzyme is a serine hydrolase responsible for degrading the fatty acid amide family of signaling lipids, including the endocannabinoid anandamide. The involvement of FAAH in pain and nervous system disorders has made it an attractive target for molecular imaging. Three [^{11}C]-labeled FAAH inhibitors have been recently reported as potential PET tracers for FAAH brain imaging (Fig. 8.3). Two were based on the irreversible covalent carbamate inhibitor URB597 (**12**) and one was based on a reversible FAAH inhibitor (MK-3168, **15**). **12** has been shown to inhibit FAAH irreversibly via carbamylation of FAAH's catalytic Ser^{241}, which acts as a nucleophile. A moderately active URB597 analog **13**

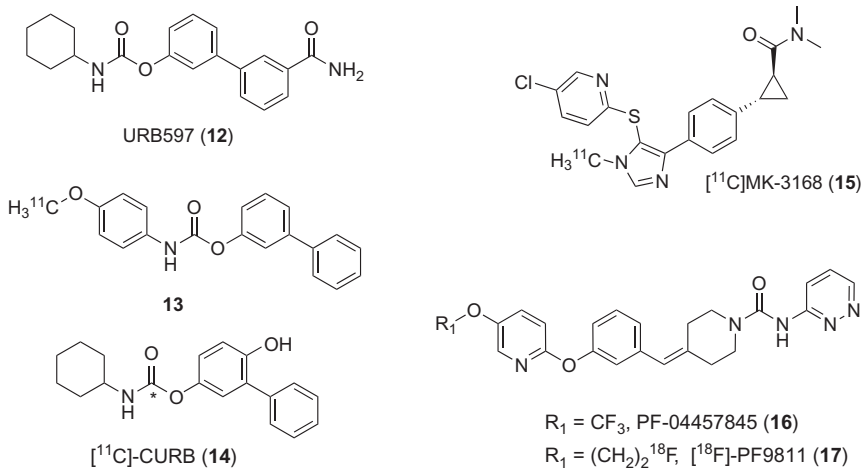

Figure 8.3 Structure of FAAH PET tracers.

($IC_{50} = 436$ nM) was targeted as a PET lead, and a [^{11}C]-methoxy group was introduced into the aniline moiety which was expected to remain attached to the enzyme upon carbamylation. Subsequent biodistribution studies showed no retention of radioactivity in brain, substantial peripheral metabolism, and minimal differences in the biodistribution patterns of wild-type and FAAH knock-out mice.[25] As a follow-up to this effort, the same group reported PET imaging results of an improved URB597 analog, [^{11}C]CURB (**14**), which was labeled at the carbonyl position using a novel [^{11}C]CO_2 fixation methodology. In contrast to the previous tracer, **14** showed heterogeneous brain binding with little washout over time which was consistent with irreversible binding. The specific binding of **14** to FAAH was demonstrated by blocking experiments with a high dose of URB597, with the highest specific binding ratio observed in cortex and the lowest in hypothalamus.[26] More recently, another novel FAAH PET tracer, [^{11}C]MK-3168 (**15**), was disclosed, which unlike previously described tracers binds to FAAH in a reversible noncovalent manner with a K_d of 0.8 nM (human cortex tissue binding). PET imaging in rhesus monkeys demonstrated heterogeneous, specific brain uptake, consistent with known regional FAAH distribution.[27] Clinical imaging studies have been carried out with **15** to provide receptor occupancy information supporting the development of a clinical candidate. Good brain uptake and test/retest variability have been reported.

Recently, our group disclosed SAR efforts in a novel urea series leading to the identification of PF-04457845 (**16**) as a clinical candidate.[28] The

excellent potency, selectivity, and pharmacokinetic properties of **16** make it an attractive scaffold for PET tracer development. Toward this end, we developed [^{18}F]PF-9811 (**17**), based on a close-in analog of **16**, wherein the trifluoromethyl moiety was replaced with a fluoroethoxy group, without impact in *in vitro* FAAH potency ($IC_{50} = 16$ nM) and *in vivo* FAAH inhibition activity (complete inhibition of FAAH *in vivo* at 10 mg/kg p.o. in C57B1/6 mice). Biodistribution experiments of **17** in rats showed good uptake in all regions of the brain, with preferential binding in the cortex, hippocampus, and cerebellum, and a statistically significant radiosignal increase from the 10 to 90-min time points, consistent with the characteristics of an irreversible inhibitor. Specificity of **17** for FAAH was demonstrated by pretreatment with **16**, which reduced uptake across all brain regions (37–73% at 90 min). In addition, **17** was evaluated in rat microPET studies and the results largely mirrored those of the biodistribution study, with high brain uptake and specific FAAH binding. The favorable outcome suggests that **17** represents a promising PET tracer for FAAH imaging with the potential advantage of a [^{18}F] radionuclide for higher resolution and flexibility in scan times.[29]

6. SPECT IN BRAIN IMAGING

SPECT has been successfully used in brain imaging, and the structures of representative clinically validated CNS SPECT tracers are shown in Fig. 8.4. The prerequisite attributes for a suitable CNS SPECT radiotracer

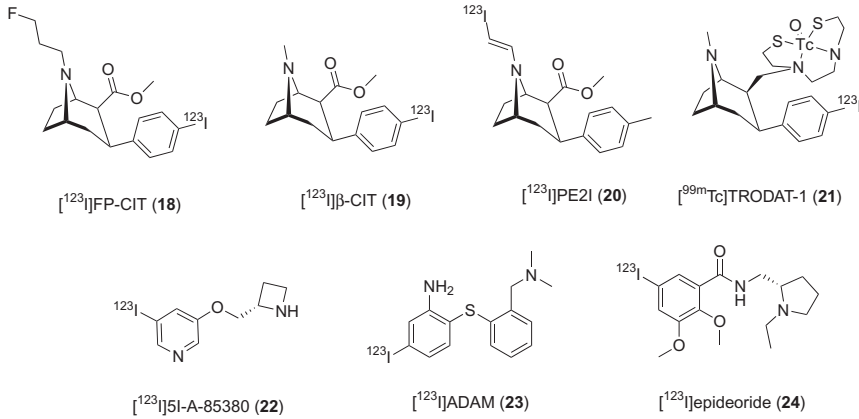

Figure 8.4 Structures of representative CNS SPECT tracers.

are similar to those of CNS PET tracers. However, there are added challenges for a SPECT tracer to meet the same set of criteria due to the nature and intrinsic properties of its radionuclides. SPECT radionuclides, such as [^{123}I] and [^{99m}Tc], are uncommon to CNS drug-like molecules, and incorporation of such radionuclides may impact physicochemical and pharmacological properties. For example, the incorporation of an [^{123}I] atom could add significant lipophilicity to the parent molecule, therefore increasing the risk of NSB. In the same way, introduction of [^{99m}Tc] would require tethering a metal complex to a small molecule, which may have significant impact on affinity for the target. Therefore, it is not surprising that most currently available CNS SPECT tracers are centered around certain type of targets, those with polar ligands which can tolerate an increase in lipophilicity (e.g., serotonin transporter, nicotinic acetylcholine receptors, and dopamine receptors) or those with high expression levels which can tolerate some loss in potency upon introduction of the SPECT radionuclide. As an example, [^{99m}Tc]-labeled CNS SPECT tracers have been successfully developed for the dopamine transporter due to the exceptionally high brain expression level of this transporter. One such example is [^{99m}Tc]TRODAT-1 (**21**), which is shown in Fig. 8.4.

Despite the limited number of clinically proven SPECT tracers available to date,[30] SPECT brain imaging studies on various neurological disorders have yielded highly impactful information and answers to important clinical neuropharmacological questions. Dopamine transporter SPECT tracers, such as [^{123}I]FP-CIT (**18**) and [^{123}I]β-CIT (**19**), are sensitive markers of dopamine neurodegeneration and have been successfully used in clinical studies to assess Parkinson's disease (PD) based on the correlation between reduction in nigrostriatal binding and disease severity.[31,2] In a recent report, SPECT imaging using **18** was also used to generate a striatal asymmetry index as a potential predictor of responsiveness to L-DOPA in patients with PD.[31] A structurally similar tracer, [^{123}I]PE2I (**20**), has shown promise as a highly sensitive and specific diagnostic tool to detect striatal neurodegeneration in patients with minor Parkinsonian symptoms.[32] SPECT tracers for other neuroreceptors have also shown promise in detecting subtle changes in receptor binding or expression levels as biomarkers for tracking various neurological disorders. For example, the nicotinic α4β2 SPECT tracer, [^{123}I]5I-A-85380 (**22**), was recently used to detect alterations in α4β2 receptor binding in patients with vascular dementia who showed decreased uptake of tracer in subcortical regions such as the dorsal thalamus and right caudate compared to age controlled healthy volunteers.[33] In similar studies,

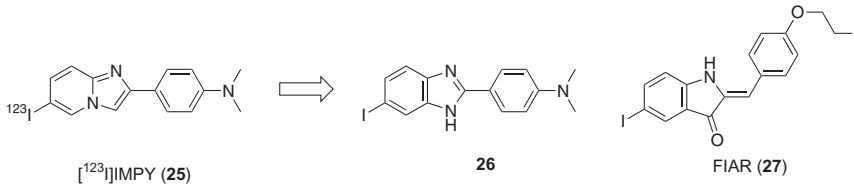

Figure 8.5 Recent disclosed SPECT tracer leads for β-amyloid plaques detection.

a serotonin transporter tracer, [^{123}I]ADAM (**23**), was used to assess the potential involvement of the mesopontine serotonergic system in the pathophysiology of migraine, revealing an increase in serotonin transporter binding in the brainstem of patients who suffer from migraines.[34] Recent publications on the development of SPECT tracers for *in vivo* detection of β-amyloid plaques are also encouraging. Two iodine-containing compounds, benzoimidazole **26** and aurone derivative FIAR **27**, were identified as improved SPECT tracer leads over [^{123}I]IMPY (**25**), the most advanced SPECT tracer for β-amyloid plaque imaging which suffers from a low signal-to-noise ratio in humans. Both compounds were reported to have high affinity for Aβ aggregates and demonstrated good signal-to-noise ratios and washout rate in mice biodistribution studies (Fig. 8.5).[35,36]

Technical advancements in the field have also dramatically improved the spatial resolution associated with SPECT measurements. For example, recently developed NanoSPECT/computed tomography (CT) can achieve resolution as low as 0.4–0.6 mm, thus allowing efficient imaging in preclinical rodent models which had been unattainable in the past.[2] This higher resolution SPECT technique could in principle be used in combination with microPET to determine the precise structural and functional anatomy of CNS disorders. The distinct advantages of SPECT in terms of cost and availability should not be overlooked. If suitable chemotypes are available and acceptable affinity can be achieved by incorporating SPECT radionuclides, development of a SPECT radiotracer should be considered as it could serve as a more economical alternative tool to PET for translational or diagnostic purposes.

7. CONCLUSIONS

In light of the considerable value of PET and SPECT brain imaging, it is important to continue to focus on the development of suitable CNS PET and SPECT tracers. A high performing PET or SPECT tracer will serve as a

powerful tool to enable clinical evaluation of candidate compounds in terms of receptor occupancy, efficacious exposures, and doses, ensuring appropriate testing of mechanisms. To enable effective decision-making in clinical studies with tracers, it will be optimal to start the tracer development early in the discovery process. Recent advances in *in vitro* screening and *in silico* tools for NSB prediction as well as tractable selection parameters for medicinal chemistry design should facilitate and accelerate the discovery process of novel CNS PET and SPECT tracers with higher success rates and fewer resources. The exciting group of new PET tracers in PDE10, ORL1, and FAAH will undoubtedly bring additional proof of the value of PET imaging in clinical validation of these hotly pursued targets. In addition, new technical advancements, particularly in SPECT, have led to better resolution/sensitivity and an expanded role in small animal preclinical imaging. Both imaging modalities, together with other imaging technologies such as CT and magnetic resonance imaging, provide an exciting translational research platform in which each of these technologies brings their unique strengths to enable high-quality preclinical and clinical studies. PET and SPECT will remain impactful technologies in the discovery of future pharmaceuticals for the treatment of neurological disorders of high unmet medical need.

REFERENCES

(1) Ametamey, S.M.; Honer, M.; Schubiger, P.A. *Chem. Rev.* **2008**, *108*, 1501.
(2) Sharma, S.; Ebadi, M. *Neurochem. Int.* **2008**, *52*, 352.
(3) Magnus, S.; Pike, V.W.; Halldin, C. *Curr. Top. Med. Chem.* **2007**, *7*, 1806.
(4) Halldin, C.; Gulyas, B.; Langer, O.; Farde, L. *Q. J. Nucl. Med.* **2001**, *45*, 139.
(5) Rahmim, A. *Iran. J. Nucl. Med.* **2006**, *14*, 1.
(6) McCarthy, D.J.; Halldin, C.; Andersson, J.D.; Pierson, M.E. *Annu. Rep. Med. Chem.* **2009**, *44*, 501.
(7) Cunningham, V.J.; Park, C.A.; Rabiner, E.A.; Gee, A.D.; Gunn, R.N. *Drug Discov. Today* **2005**, *2*, 311.
(8) Van de Waterbeemd, H.; Camenisch, G.; Folkers, G.; Chretien, J.; Raevsky, O. *J. Drug Target* **1998**, *6*, 151.
(9) Guo, Q.; Brady, M.; Gunn, R.N. *J. Nucl. Chem.* **2009**, *50*, 1715.
(10) Jiang, Z.J.; Reilly, J.; Everatt, B.; Briard, E. *J. Pharm. Biomed. Anal.* **2011**, *54*, 722.
(11) Rosso, L.; Gee, A.D.; Gould, I.R. *J. Comput. Chem.* **2008**, *29*, 2397.
(12) Dickson, C.J.; Gee, A.D.; Bennacef, I.; Gould, I.R.; Rosso, L. *Phys. Chem. Chem. Phys.* **2011**, *13*, 21552.
(13) Tavares, A.A.S.; Lewsey, J.; Dewar, D.; Pimlott, A.L. *Nucl. Biol. Med.* **2012**, *39*, 127.
(14) Zhang, L.; Villalobos, A.; Anderson, D.; Beck, E.; Blumberg, L.; Bocan, T.; Bronk, B.; Chen, L.; Brown-Proctor, C.; Grimwood, A.; Heck, S.; Skaddan, M.; McCarthy, T.; Zasadny, K. *J. Labelled Comp. Radiopharm.* **2011**, *54*, S292.
(15) Wager, T.; Hou, X.; Verhoest, P.; Villalobos, A. *ACS Chem. Neurosci.* **2010**, *1*, 435.
(16) Wager, T.; Chandrasekaran, R.Y.; Hou, X.; Troutman, M.D.; Verhoest, P.R.; Villalobos, A.; Will, Y. *ACS Chem. Neurosci.* **2010**, *1*, 420.
(17) Tu, Z.; Xu, J.; Jones, L.A.; Li, S.; Mach, R.H. *Nucl. Med. Biol.* **2010**, *37*, 509.

(18) Tu, Z.; Fan, J.; Li, S.; Jones, L.A.; Cui, J.; Padakanti, P.K.; Xu, J.; Zeng, D.; Shoghi, K.I.; Perlmutter, J.S.; Mach, R.H. *Bioorg. Med. Chem.* **2011**, *19*, 1666.
(19) Plisson, C.; Salinas, C.; Weinzimmer, D.; Labaree, D.; Lin, S.-F.; Ding, Y.-S.; Jakobsen, S.; Smith, P.W.; Eiji, K.; Carlson, R.E.; Gunn, R.N.; Rabiner, E.A. *Nucl. Med. Biol.* **2011**, *38*, 875.
(20) Celen, S.; Koole, M.; Angelis, M.D.; Sannen, I.; Chitneni, S.K.; Alcazar, J.; Dedeurwaerdere, S.; Moechars, D.; Schmidt, M.; Verbruggen, A.; Langlois, X.; Laere, K.V.; Andres, J.I.; Bormans, G. *J. Nucl. Med.* **2010**, *51*, 1584.
(21) Andres, J.-I.; Angelis, M.D.; Alcazar, J.; Iturrino, L.; Langlois, X.; Dedeurwaerdere, S.; Lenaerts, I.; Vanhoof, G.; Celen, S.; Bormans, G. *J. Med. Chem.* **2011**, *54*, 5820.
(22) Hostetler, E.; Cox, C.D.; Fan, H. WO 2010138577, **2010**.
(23) Pike, V.W.; Rash, K.S.; Chen, Z.; Pedregal, C.; Statnick, M.A.; Kimura, Y.; Hong, J.; Zoghbi, S.S.; Fujita, M.; Toledo, M.A.; Diaz, N.; Gackenheimer, S.L.; Tauscher, J.T.; Barth, V.N.; Innis, R.B. *J. Med. Chem.* **2011**, *54*, 2687.
(24) Hostetler, E.; Sanabria-Bohorquez, S.; Eng, W.S.; Joshi, A.; Gibson, R.; Patel, S.; O'Malley, S.; Krause, S.; Ryan, C.; Riffel, K.; Okamoto, O.; Ozaki, S.; Ohta, H.; Cook, J.; Burns, H.D.; Hargreaves, R. *J. Labelled Comp. Radiopharm.* **2011**, *54*, S78.
(25) Wyffels, L.; Muccioli, G.G.; Kapanda, C.N.; Labar, G.; Bruyne, S.D.; Vos, F.D.; Lambert, D.M. *Nucl. Med. Biol.* **2010**, *37*, 665.
(26) Wilson, A.A.; Garcia, A.; Parkes, J.; Houle, S.; Tong, J.; Vasdev, N. *Nucl. Med. Biol.* **2011**, *38*, 247.
(27) Li, W.; Sanabria-Bohórquez, S.; Joshi, A.; Cook, J.; Holahan, M.; Posavec, D.; Purcell, M.; DeVita, R.; Chobanian, H.; Liu, P.; Chioda, M.; Nargund, R.; Lin, L.; Zeng, Z.; Miller, P.; Chen, T.; O'Malley, S.; Riffel, K.; Williams, M.; Bormans, G.; Van Laere, K.; De Groot, T.; Evens, N.; Serdons, K.; Depre, M.; de Hoon, J.; Sullivan, K.; Hajdu, R.; Shiao, L.; Alexander, J.; Blanchard, R.; DeLepeleire, I.; Declercq, R.; Hargreaves, R.; Hamill, T. *J. Labelled Comp. Radiopharm.* **2011**, *54*, S38.
(28) Johnson, D.S.; Stiff, C.; Lazerwith, S.E.; Kesten, S.R.; Fay, L.K.; Morris, M.; Beidler, D.; Liimatta, M.; Smith, S.E.; Dudley, D.T.; Sadagopan, N.; Bhattachar, S.N.; Kesten, S.J.; Nomanbhoy, T.K.; Cravatt, B.F.; Ahn, K. *ACS Med. Chem. Lett.* **2011**, *2*, 91.
(29) Skaddan, M.B.; Zhang, L.; Johnson, D.S.; Zhu, A.; Zasadny, K.; Coelho, R.V.; Kuszpit, K.; Currier, G.; Fan, K.-H.; Beck, E.; Chen, L.; Drozda, S.E.; Balan, G.; Niphakis, M.; Cravatt, B.F.; Ahn, K.; Bocan, T.; Villalobos, A. *Nucl. Med. Biol.*, **2012**, *in press*.
(30) Gomes, C.M.; Abrunhosa, A.J.; Ramos, P.; Pauwels, E.K.J. *Adv. Drug Delivery Rev.* **2011**, *63*, 547.
(31) Contrafatto, D.; Mostile, G.; Nicoletti, A.; Raciti, L.; Luca, A.; Dibilio, V.; Lanzafame, A.; Distefano, A.; Drago, F.; Zappia, M. *Clin. Neuropharmacol.* **2011**, *34*, 71.
(32) Ziebell, M.; Andersen, B.B.; Thomsen, G.; Pinborg, L.H.; Karlsborg, M.; Hasselbalch, S.G.; Knudsen, G.M. *Eur. J. Nucl. Med. Mol. Imaging* **2012**, *39*, 242.
(33) Colloby, S.J.; Firbank, M.J.; Pakrasi, S.; Perry, E.K.; Pimlott, S.L.; Wyper, D.J.; McKeith, I.G.; Williams, E.D.; O'Brien, J.T. *Neurobiol. Aging* **2011**, *32*, 293.
(34) Schuh-Hofer, S.; Richter, M.; Geworski, L.; Villringer, A.; Israel, H.; Wenzel, R.; Munz, D.L.; Arnold, G. *J. Neurol.* **2007**, *254*, 789.
(35) Chu, M.; Ono, M.; Kimura, H.; Kawashima, H.; Liu, B.L.; Saji, H. *Nucl. Med. Biol.* **2011**, *38*, 313.
(36) Watanabe, H.; Ono, M.; Kimura, H.; Kagawa, S.; Nishii, R.; Fuchigami, T.; Haratake, A.; Nakayama, M.; Saji, H. *Bioorg. Med. Chem. Lett.* **2011**, *21*, 6519.